Title
Critical Parameter Identification of Fuel-Cell Models Using Sensitivity Analysis

Journal
Journal of The Electrochemical Society, 168(7)

ISSN
0013-4651

Authors
Pant, Lalit M
Stewart, Sarah
Craig, Nathan
et al.

Publication Date
2021-07-01

DOI
10.1149/1945-7111/ac0d68

Peer reviewed

Critical Parameter Identification of Fuel-Cell Models Using Sensitivity Analysis

Journal of The Electrochemical Society, 2021 **168** 074501

Critical Parameter Identification of Fuel-Cell Models Using Sensitivity Analysis

Lalit M. Pant,[1,*,z] Sarah Stewart,[2] Nathan Craig,[2] and Adam Z. Weber[1,]**

[1]*Energy Conversion Group, Energy Technologies Area, Lawrence Berkeley National Laboratory, Berkeley, California 94720, United States of America*
[2]*Robert Bosch LLC, Sunnyvale, California 94085, United States of America*

Numerical modeling has been a vital tool in proton-exchange-membrane fuel-cell (PEMFC) analysis; however, the predictive capabilities of these models depend on the input physical parameters, several of which are either not experimentally measured or have large scatter in measured values. This article presents an uncertainty propagation-based sensitivity analysis to identify the model parameters that impact the model predictions most. A comprehensive 2-D membrane electrode assembly (MEA) model is used to perform local sensitivity analysis at multiple operating conditions, which encompass the range of environments and operating conditions a cell can encounter. While at lower humidities, cathode kinetics and membrane-ohmic-loss related parameters are crucial, gas transport and porous-media saturation behavior are more important at humidified conditions. Several of these findings are different from previous studies presented in literature. Identifying the crucial parameters helps focus future material and cell optimization studies as well as experimental studies to quantify these parameters with higher accuracy.
 [DOI: 10.1149/1945-7111/ac0d68]

Manuscript submitted January 24, 2021; revised manuscript received June 7, 2021. Published July 5, 2021. *This was paper 1596 presented during PRiME 2020, October 4–9, 2020.*

Supplementary material for this article is available online

Proton-exchange-membrane fuel cells (PEMFCs) are a promising energy-conversion technology for the 21st century; however, further improvements in performance and durability are required for large scale commercialization of this technology.[1] Modeling, especially continuum modeling has been vital in providing insights on phenomena governing cell-level performance.[2–4] A variety of continuum models have been developed and used in literature.[5–18] The accuracy and predictive power of these models is dependent upon the implemented physics and the associated parameters. A majority of the work in literature has focused on improving the accuracy and complexity of the implemented physics, where models with higher dimensions,[10,11,16,17] non-isothermal and two-phase physics,[9] more rigorous kinetics,[19,20] and other improvements have been developed.[2] However, there has been little work on understanding the effect of model parameters on the accuracy and predictive power of mathematical models[21–23] even though these validated models can provide material design, integration, and optimization guidance.

Vetter and Schumacher[24] recently presented a through literature review of the parameters used in PEMFC models. A significant spread is observed in the measurements of properties such as membrane water uptake, membrane conductivity, porous-media transport parameters, etc. In addition, certain parameters such as evaporation rates and membrane adsorption/desorption rates are not known accurately, with assumptions spanning several orders of magnitude. Vetter and Schumacher[24] also showed that these uncertainties in input parameters lead to significant variations in model predicted cell polarization curves. It is worth noting that a parameter that is crucial in one modeling framework may not be so important in a different model. However, for any model, it is important to understand the impact of modeling parameters on its predictions, i.e., the sensitivity of the model outputs towards its input parameters must be identified.

Sensitivity analysis-based parameter estimation has been prevalent in battery modeling.[25–27] Initial sensitivity analysis on PEMFC models has also focused on model parameter estimation.[28,29] Later PEMFC sensitivity analyses have been focused on understanding impact of model parameters' uncertainty on model predictions.[22,23,30–40] However, these models have either been empirical stack based models or simplistic cell models and therefore have not been able to elucidate the issues in detailed physics-based models. Vetter and Schumacher[41] recently presented one of the first PEMFC sensitivity analysis on a complete 1-D multi-physics model. While the article presented a valuable framework and a thorough analysis of parameter uncertainty impacts, the model still did not encompass the complete complexity of membrane-electrode-assembly (MEA) physics, e. g., coupled water and proton transport in membrane, agglomerate effects in cathode, etc. Furthermore, the 1-D model was not able to account for land-channel effects or along-the-channel impacts. Recently, Goshtasbi, et al.[21,42] presented a detailed sensitivity analysis that focused on estimating cell parameters from simple polarization-curve data. While the analysis itself was thorough, the MEA physics was simplified to account for along-the-channel effects.

This article presents a detailed sensitivity analysis based on framework using our previously developed comprehensive 2-D MEA model.[18] Compared to the other models used in sensitivity analysis, this model accounts for detailed macroscale physics and therefore is capable of providing a better insight on the impact of different physical parameters on model predictions. The rest of the article is organized as follows: the next section presents the methodology used for cell modeling and sensitivity analysis, followed by evaluation of the parameter sensitivity in 2-D model. Finally, the article summary and conclusion are presented.

Methodology

PEMFC modeling.—An in-house developed 2-D MEA model is used for simulating PEMFC performance.[15,18] Figure 1 shows the schematic of the simulation domain used. While the detailed description of the model is presented by Pant, et al.,[18] a brief summary and unique parameters are discussed in the following paragraphs. Pant, et al.[18] have shown both: a 2-D model and a pseudo-3D (1+2D) model, but this article only utilizes the 2-D model, as using the pseudo 3-D model for sensitivity analysis is currently computationally costly compared to the benefits since the governing physics and phenomena are well captured by the 2-D model itself.

A steady-state, macro-homogeneous, multiphase and multiphysics modeling approach is used with spatially volume averaged

*Electrochemical Society Member.
**Electrochemical Society Fellow.
[z]E-mail: LMPant@lbl.gov

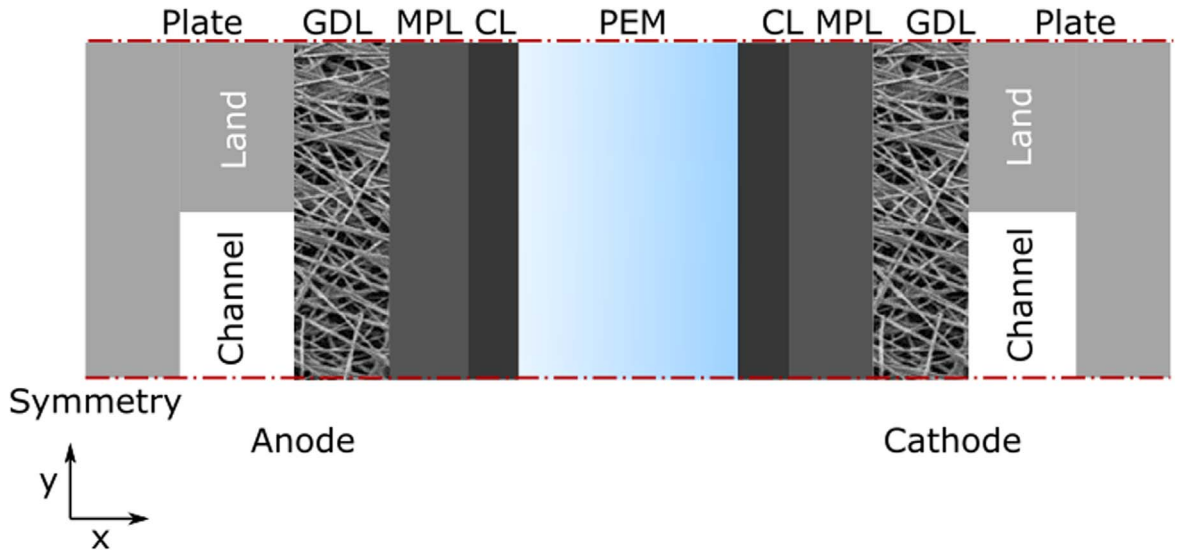

Figure 1. Schematic of the modeling domain of a 2-D MEA cross-section. Image not to scale.

effective properties of each layer. The model accounts for multi-component gas diffusion, liquid and gas convection, electron transport, heat transport, and proton & water transport in ionomer in the catalyst layers and membrane. The anode hydrogen-oxidation reaction (HOR) is modeled using a Butler-Volmer reaction.[18] The cathode oxygen-reduction reaction (ORR) is modeled using a Tafel equation combined with an agglomerate modeling approach.[18] To understand the impact of reaction order on sensitivity, reaction orders are varied over a range for ORR. Since the conventional agglomerate formulation is only applicable for first order ORR,[20,43,44] a semi-analytical formulation is used to enable one to examine the impact of different reaction orders;[43] an overview of the agglomerate-based cathode kinetics model is provided in supplementary material section 1.

Sensitivity analysis.—To understand the sensitivity of a function or model to its input parameters, a condition number can be utilized, which is frequently applied in linear algebra and regression analysis.[45,46] The cell model can be approximated as a model function from an n- dimensional input space to an m-dimensional output space ($\vec{f}: \mathbb{R}^n \rightarrow \mathbb{R}^m$). The sensitivity of any i^{th} output of $\vec{f}$ with respect to j^{th} input (x_j) is then obtained with the relative condition number, defined as[41,45,46]

$$\kappa_{ij}(\vec{x}) = \left| \frac{\partial \log f_i(\vec{x})}{\partial \log x_j} \right| = \left| \frac{x_j}{f_i(\vec{x})} \frac{\partial f_i(\vec{x})}{\partial x_j} \right|. \quad [1]$$

Where $\vec{x} = \{x_1, x_2, x_3, \cdots, x_n\}$ is a sample point in the n-dimensional input space and f_i is the i^{th} output in the m-dimensional output space.[a] For a non-differentiable function, the relative condition number can be defined as[41]

$$\kappa_{ij}(\vec{x}) = \lim_{\delta \to 0} \sup_{|\Delta x_j| \leqslant \delta} \left| \frac{x_j}{f_i(\vec{x})} \frac{f_i(\vec{x} + \Delta x_j \vec{e}_j) - f_i(\vec{x})}{\Delta x_j} \right|, \quad [2]$$

where $\vec{e}_j$ is the unit vector for j^{th} parameter and Δx_j is the magnitude of perturbation in the j^{th} parameter. The relative condition number can be thought of as the uncertainty amplification/dampening factor from input to output. For example, if the j^{th} input changes by $x\%$, then the i^{th} output will change by $x\kappa_{ij}\%$. If κ_{ij} is large, then the output f_i is sensitive to input x_j and vice versa.

For implementation purpose, Vetter and Schumacher[41] suggested to fix $\Delta x_j = \delta x_j$ and keeping δ very small. Equation 2 can be then expressed as

$$\kappa_{ij}(\vec{x}) \simeq \frac{1}{\delta} \left| \frac{f_i(\vec{x} + \delta x_j \vec{e}_j)}{f_i(\vec{x})} - 1 \right|. \quad [3]$$

κ_{ij} is not only an uncertainty propagation factor in the model, it can also be used for optimization purposes. For this, not only the magnitude of κ_{ij} is necessary but also the sign is needed. Therefore, in this article, κ_{ij} is redefined as

$$\kappa_{ij}(\vec{x}) \simeq \frac{1}{\delta} \left(\frac{f_i(\vec{x} + \delta x_j \vec{e}_j)}{f_i(\vec{x})} - 1 \right). \quad [4]$$

Assuming that the model represents the physical system accurately, κ_{ij} can be used to understand whether an input can be changed to affect an output in a desired way. For example, if κ_{ij} is positive then increasing x_j will increase f_i as well.

For sensitivity analysis, first the output variables need to be selected. In this article, variables that are representative of the cell's performance and internal state are used. For this purpose, cell current (i_{cell}), minimum water content in ionomer ($\lambda_{\min}$), average water content in ionomer (λ_{av}), maximum cell temperature ($T_{\max}$), minimum overpotential ($\eta_{\min}$), maximum overpotential ($\eta_{\max}$), and maximum liquid saturation in all porous layers ($S_{L,\max}$) are used. While most of these variables except cell current (i_{cell}) are not directly measurable, they can be inferred from other measurements such as HFR, cell water balance and cell/coolant temperature. Even though these variables are not directly measurable, they convey crucial information about cell health/state and are composite parameters depending on several measurable properties. The relevance of each of these output variables is discussed in Table I. The cell model can be simulated in both: potentio-static (fixed potential) and galvano-static (fixed current) modes. While galvano-static mode allows one to control the water production and therefore hydration state of cell, the potentio-static mode controls the overpotentials. Furthermore, given that this article is focused on steady-state performance, galvano-dynamic simulations are beyond the scope of current work. To ensure that the cell's sensitivity is evaluated in the three main operating regimes: kinetics, ohmic and transport limited, the model is simulated at potentio-static conditions and output variables are evaluated at three potentials: 0.8, 0.67, and

[a]For example, think of a cell simulation model function which computes cell current (i_{cell}) and average membrane water content ($\bar{\lambda}$) as a function of cell temperature (T) and cell voltage (V). Then the function can be defined as $\vec{f}: \mathbb{R}^2 \rightarrow \mathbb{R}^2$. A sample point $\vec{x}$ is a given temperature and cell voltage ($\vec{x} = \{T_l, V_m\}$). Sensitivity of average membrane water content with respect to temperature at the sample point can be obtained as: $\kappa_{\bar{\lambda}T} = \frac{\partial \log \bar{\lambda}(T_l, V_m)}{\partial \log T}$

Table I. Relevance of the selected output variables for cell health analysis.

Output	Relevance
i_{cell}	Cell performance
$\lambda_{\min}$	State of driest parts of membrane
λ_{av}	Average membrane hydration
$T_{\max}$	Cell overheating
$\eta_{\min}$	Catalyst layer utilization
$\eta_{\max}$	Catalyst layer utilization
$S_{L,\max}$	Electrode flooding condition

0.3 V. These potentials are also consistent with Department of Energy's benchmarking conditions for low-temperature fuel cells.[47] Overall, 21 (7 × 3) output variables are evaluated for sensitivity analysis of the model.

Table A·I shows the input parameters used in this article, with respect to which the sensitivities of the output variables are evaluated. Either the values of inputs themselves are changed or the inputs are adjusted using a pre-factor. The definition of the parameters is consistent with the original model as described by Pant, et al.[18] Overall, the sensitivity is analyzed with respect to operating conditions and geometric, kinetics, and transport parameters. Given the number of input parameters, a true global sensitivity analysis would be infeasible. Therefore, local sensitivity analysis is performed in which a single parameter is varied at a time while keeping the rest at a fixed value. To account for the cell operation at different conditions, the sensitivity analysis is performed at six operating conditions: 80 °C, 80%RH, air, 150 kPa; 80 °C, 40% RH, air, 150kPa; 80 °C, 100%RH, air, 150 kPa; 80 °C, 80% RH, 5% O2, 150 kPa; 80 °C, 80%RH, air, 250 kPa; and 95 °C, 80%RH, air, 250 kPa, which represent normal, dry, flooded, fuel-starved, high-back pressure, and heavy-duty conditions. Overall, 18 base-case studies (3 potentials × 6 operating conditions) are performed.

Results and Discussion

For every operating condition, each sensitivity parameter is varied within the range specified in Table A·I, while the remaining parameters are fixed at their base value. The range of values is chosen based on the spread observed in literature. The base values of all the parameters and operating conditions are given in Table SI (supplementary information). The model is implemented in COMSOL™ framework and cell operation is simulated at given parameters. At any given parameter value, the sensitivity is obtained by perturbation analysis as shown in Eq. [4]. For each parameter, except layer thickness, sensitivity evaluation is done at 40 uniformly distributed intermediate points between minimum and maximum value of the parameter. For thickness, only 10 points are evaluated due to higher computational time. The overall computation time for sensitivity analysis of all parameters at a given operating condition is approximately 84 h. Figure 2A shows an example of sensitivity of cell current at 0.3 V towards gas diffusion layer (GDL) porosity for a cell at 80 °C, 40% RH, 150kPa cell pressure, and air cathode. The sensitivity towards a parameter can be positive and/or negative depending on different system behavior at different parameter values. For example, at lower GDL porosity the cell is limited by oxygen transport at high current densities (0.3 V), therefore an increase in the porosity results in increased transport and therefore shows a positive sensitivity. For high GDL porosity however, oxygen transport is not limiting. Instead, higher GDL diffusion leads to more water diffusing outwards from the catalyst layers, leading to membrane dehydration and a reduction in cell current densities; therefore, it exhibits a negative sensitivity.

For faster analysis and easier comparison of sensitivity between different input-output pairs, each sensitivity profile is converted into a heatmap. The heatmap equivalent of Fig. 2(A) is shown in Fig. 2B. The heatmap is generated by plotting the log of the sensitivity magnitude. Positive sensitivity values are plotted in blue color at the center and negative sensitivities are plotted in red color towards the outer edge. The intensity of the color represents the log magnitude as shown in the colorbar. Figure 2C shows the complete map of the sensitivity of the different model outputs to the most sensitive input parameters. The heatmap provides ways for analysis, discussion and importance ranking of each input-output pair; however, since evaluating exact values in heatmaps is difficult, the readers are referred to supplementary material for detailed plots of sensitivity for each parameter. Detailed sensitivity plots for each input parameter at 80 °C, 40% RH, 150kPa cell pressure, and air are given in supplementary information Figs. S1-S6 (available online at stacks.iop.org/JES/168/074501/mmedia).

For an air-based cell at 80 °C, 40% RH, several model parameters exhibit significant impact on the model outputs. As expected, the model is sensitive to cathode kinetics parameters due to slow ORR, especially to the cathodic transfer coefficient. Anode kinetics plays a minor role and is sensitive only when the anode kinetics is slowed by an order of magnitude with respect to reference value (see Fig. S1a). Due to dry conditions (40% RH), membrane hydration is low and therefore ionomer properties related to proton conduction show significant impact on the outputs. The model outputs also exhibit sensitivity to cell geometry at these conditions. An increase in cathode catalyst layer (CL) thickness improves performance due to increased electrochemically active surface area (ECSA) and increasing membrane thickness shows negative impact due to increased ohmic losses. The cell performance also shows significant sensitivity to operating conditions, e.g., cell temperature and humidity. While cell conditions are usually measured accurately during experimentation, several issues such as location of thermocouple, feedline insulation, cooling system efficiency, etc can cause the operating conditions within cell to be different than the measured values. Given the high sensitivity of model outputs towards the operating conditions, this can cause large discrepancies between model predictions and experimental data, which can cast an unnecessary doubt in the model capabilities even though the errors are due to incorrect input parameters.

To understand the impact of a particular sensitivity magnitude on cell performance, polarization curves are simulated with varying values of sensitive parameters. Figure 3 shows the impact of varying cathode ECSA ($A_{v,c}$) and ORR cathodic transfer coefficient ($\alpha_{c,ORR}$) by 10% and 50%. Figures S1f and S1h show the sensitivity of model outputs to these parameters. Since the impact is analyzed in comparison to reference values, we are primarily concerned with the sensitivity of these parameters at relative values (with respect to reference) near 1. While the sensitivity of cell current with respect to $\alpha_{c,ORR}$ is between 2 to 6 near the reference value, the sensitivity with respect to $A_{v,c}$ is lower (closer to 0.25 to 0.75). It can therefore be seen in Fig. 3 that at 0.3 V, changing the $\alpha_{c,ORR}$ by 10% results in a current change by approximately 50% (~5 × 10), while changing $A_{v,c}$ by same amount increases the current by only 7% (~0.7 × 10). This shows that even a small uncertainty in the input parameters can result in significant output changes for sensitive parameters. To achieve the same amount of impact on the polarization behavior for less sensitive parameters requires a much higher perturbation range; however, as discussed earlier, uncertainties of several orders of magnitudes exist for some input parameters that can significantly impact the model outputs.

Next, the model sensitivity was analyzed at 80 °C, 80% RH, 150 kPa cell pressure, and air cathode to understand the model behavior at more humid conditions (referred here as standard conditions). Figure 4 shows the sensitivity heatmap of the model for the most sensitive parameters. Detailed sensitivity analysis for all parameters at 80 °C, 80% RH, 150 kPa cell pressure, and air are given in supplementary information Figs. S7–S12. The kinetics and ionomer properties exhibit similar behavior as in 80 °C and 40% RH case, as slow ORR and ionomer proton conduction are still an issue

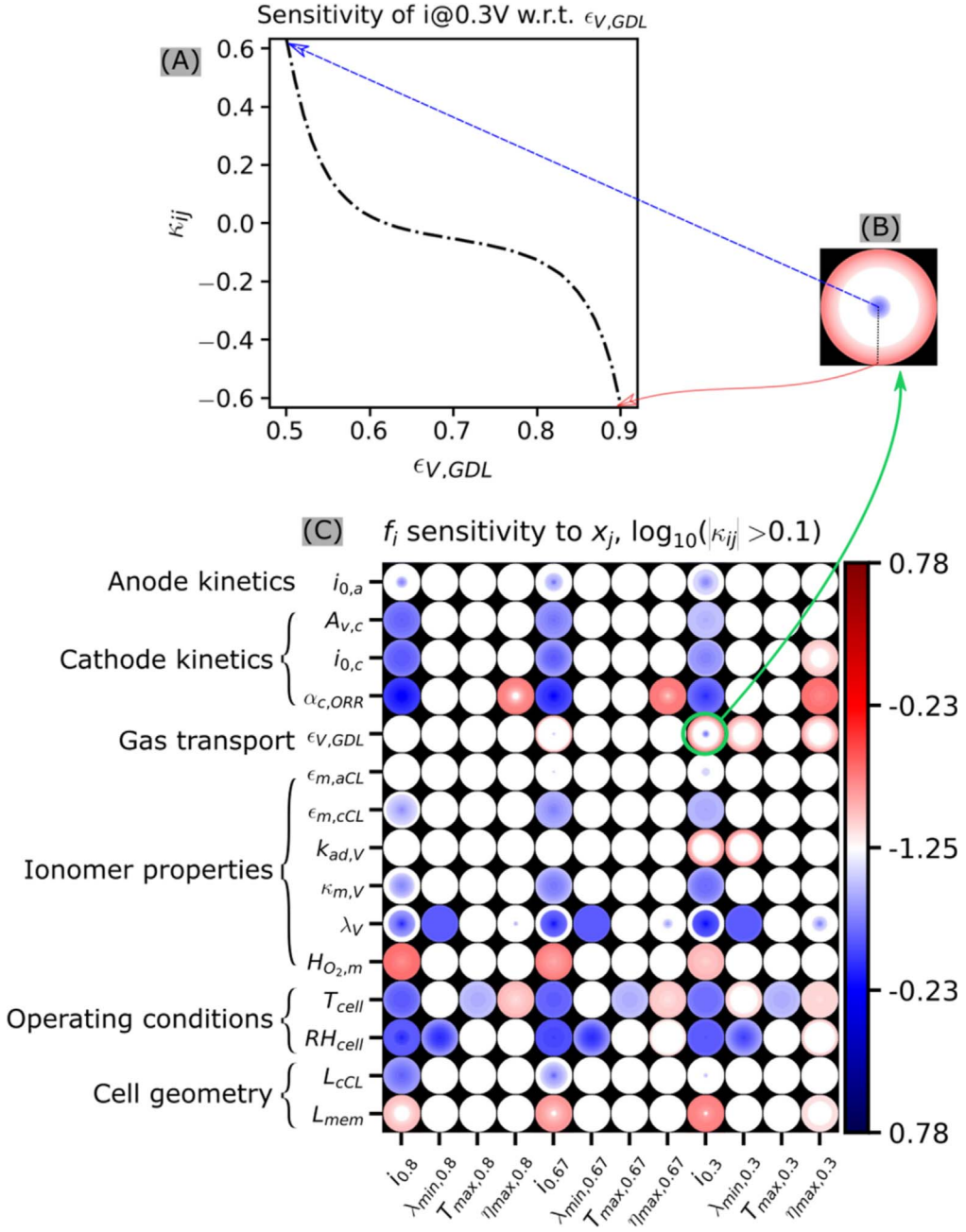

Figure 2. Sensitivity analysis of the model at 80 °C, 40% RH (dry conditions), 150kPa cell pressure, and air. (a) An example of complete sensitivity profile of a single input-output pair showing sensitivity of cell current at 0.3 V towards GDL porosity, (b) Representation of the same sensitivity profile as a heatmap. Blue colour represents positive sensitivity values (+ve κ_{ij}) and red colour represents negative sensitivity values (−ve κ_{ij}). The centre of the circular grid shows the maximum positive sensitivity, and the edges shows the maximum negative sensitivity, (c) Sensitivity map of the model outputs with respect to the most sensitive model inputs. The heatmap shows logarithmic values of the sensitivity magnitude. The parameters are defined in Table A·I.

at 80% RH. However, unlike at the drier conditions, the partial pressure of O_2 is lower due to higher humidity. This results in some of the GDL gas-transport parameters and ORR order also becoming critical parameters. The thermal properties of GDL, micro-porous layer (MPL) and coolant also impact the model output, especially at higher current densities. Most of the heat in PEMFCs is generated in the membrane and CLs due to ohmic heating and reactions. The thermal properties of GDL, MPL and coolant control the rate of heat escape and therefore the CL local temperature. This in turn affects the local water activity and membrane hydration, especially at near saturation conditions, which exist at high humidity and high current-density operation.

To further understand the effect of operating conditions on model sensitivity, analysis was performed at oxygen starved conditions: 80 °C, 80% RH, 150 kPa cell pressure, and 5% O_2 in the cathode. This condition represents an oxygen starved cell, which can occur during low stoichiometry operation or at channel exits. Figure 5 shows the sensitivity heatmap of the model for the most sensitive parameters in this condition. A detailed sensitivity analysis with respect to each parameter is shown in supplementary information Figs. S13–S18. The sensitivity behavior of most parameters is similar to the sensitivity map shown in Fig. 4 for higher O_2 concentration. Due to the oxygen-starved conditions, reaction order (γ_{O_2}) demonstrates a much higher impact on cell performance

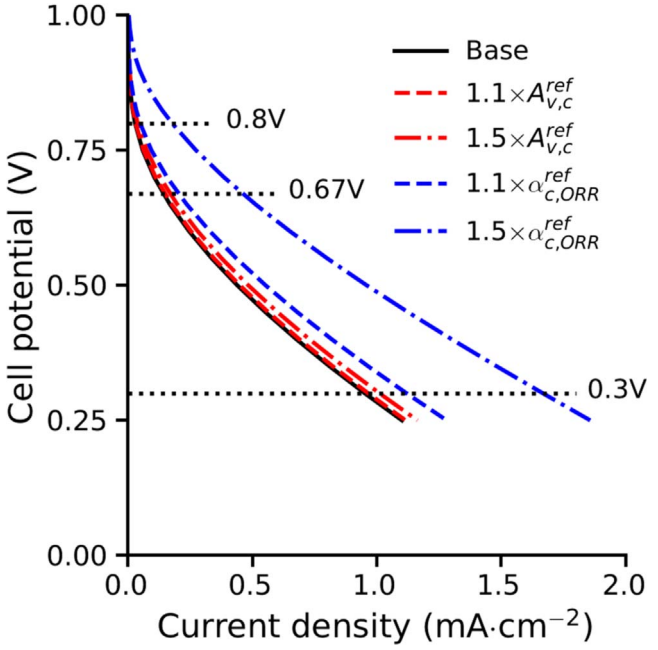

Figure 3. Impact of varying cathode ECSA ($A_{v,c}$) and ORR cathodic transfer coefficient ($\alpha_{c,ORR}$) by 10% and 50% on cell performance at 80 °C, 40%RH (dry conditions), 150 kPa cell pressure, and air cathode. The base curve uses reference properties described in Table SI.

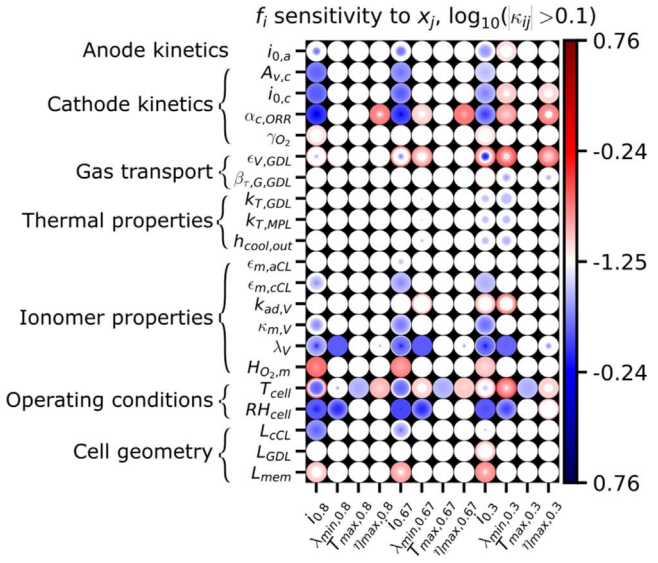

Figure 4. Sensitivity analysis heatmap of the model at 80 °C, 80% RH (standard conditions), 150 kPa cell pressure, and air. The heatmap shows logarithmic values of the sensitivity magnitude. The parameters are defined in Table A·I.

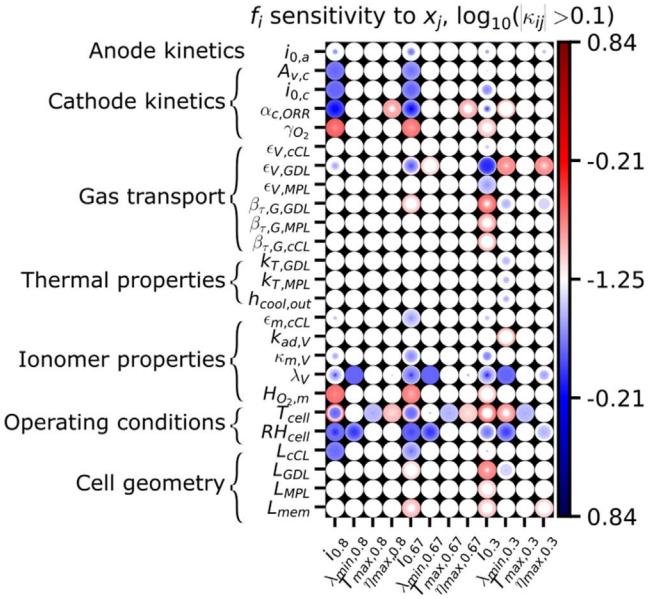

Figure 5. Sensitivity analysis heatmap of the model at 80 °C, 80% RH, 150kPa cell pressure, and 5% O2 in cathode (oxygen starved). The heatmap shows logarithmic values of the sensitivity magnitude. The parameters are defined in Table A·I.

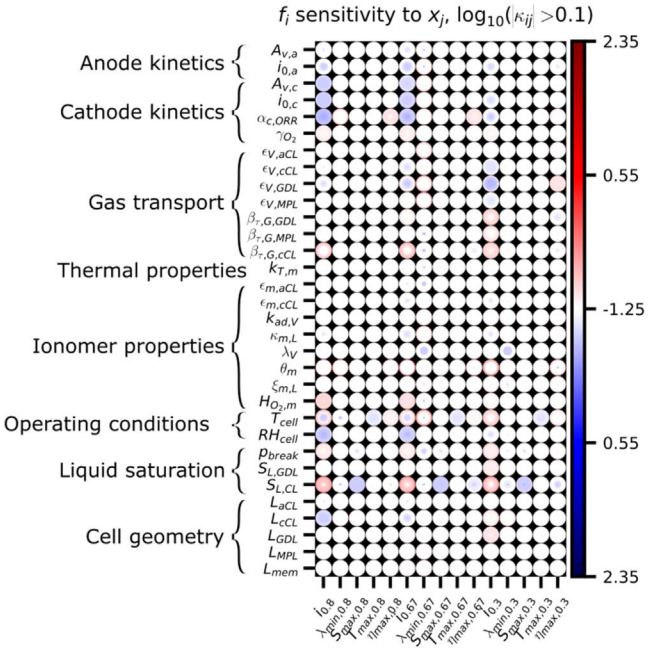

Figure 6. Sensitivity analysis heatmap of the model at 80 °C, 100% RH (flooded condition), 150 kPa cell pressure, and air in cathode. The heatmap shows logarithmic values of the sensitivity magnitude. The parameters are defined in Table A·I.

compared to the air-fed cathode. Not only do the GDL transport properties show higher sensitivity compared to Fig. 4, transport properties of MPL and cathode CL, which were not crucial for air-fed cell, also show an appreciable impact on cell performance. The thicknesses of all the porous layers are also important in this case, as increasing thickness increases the transport losses, which impacts the cell performance significantly in an already reactant-starved cell.

To understand the cell behavior at saturated conditions, the model sensitivity was analyzed at 80 °C, 100% RH, 150 kPa cell pressure, and air in the cathode. Figure 6 shows the sensitivity analysis heatmap of the model for the most sensitive parameters. The detailed sensitivity analysis for each parameter is given in supplementary material Figs. S19–S24. While the maximum sensitivity of the model outputs towards any input parameter is in the range of $10^{0.7}-10^{0.9}$ for non-flooded conditions, it can be seen in Fig. 6 that for saturated conditions, some parameters show much higher sensitivity value—in the order of $10^{2.35}$. Furthermore, a significantly higher number of input parameters become impactful for the model predictions at saturated conditions. Due to flooded conditions, reactant transport becomes a limiting factor in both cathode and anode. Due to low reactant concentration in the CL, the model displays sensitivity to both anode and cathode kinetic

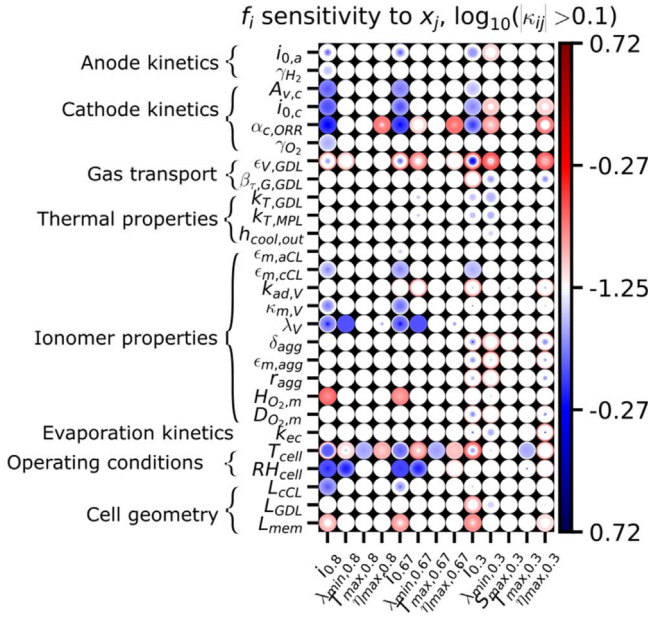

Figure 7. Sensitivity analysis heatmap of the model at 95 °C, 80% RH (heavy duty condition), 250kPa cell pressure, and air in cathode. The heatmap shows logarithmic values of the sensitivity magnitude. The parameters are defined in Table A·I.

parameters. In terms of gas transport, it is seen that transport properties of all porous layers in cathode and anode show impact on the model outputs at 100% RH, while in dry conditions only cathode was crucial, as the anode is only transport limited at 100% RH. Similarly, thicknesses of all layers become critical as they contribute to the transport resistance. Due to the fully humidified conditions, the liquid-equilibrated ionomer properties also exhibit impact on the outputs, while for drier conditions, only the vapor-equilibrated ionomer properties were crucial. Finally, saturation characteristics of the GDL and catalyst layers also become critical as they control the liquid saturation and thus the effective transport properties.

All the aforementioned studies were conducted at a cell pressure of 150 kPa in both anode and cathode. To understand the impact of cell pressure, sensitivity analysis was also performed at 80 °C, 80% RH, air in cathode and 250 kPa cell pressure. The heatmap (Fig. S25) and detailed plots are provided in the supplementary material (Figs. S26–S31). Overall, no major difference was seen in sensitivity profile at 250 kPa (Fig. S25) compared to the one at 150 kPa (Fig. 4). This suggests that at the given operating conditions, cell pressure, which is primarily a surrogate for reactant concentration, is not as crucial, as oxygen concentration is not limiting. This will be different when operating at low oxygen mole fractions as shown earlier in 5% O_2 analysis.

Recently there has been a lot of interest in using PEMFCs for heavy duty vehicles. For performance and efficiency considerations, these cells usually operate at higher temperatures and pressures. To understand the cell behavior at such conditions, sensitivity analysis was performed at 95 °C, 80%RH, air in cathode and 250 kPa cell pressure. Figure 7 shows the sensitivity analysis heatmap for the most sensitive parameters. The detailed sensitivity analysis for each parameter is given in supplementary material Figs. S32–S37. Compared to the 80 °C, 80%RH case shown in Fig. 4, the sensitivity map at 95 °C, 80%RH looks similar. Agglomerate properties and evaporation/condensation coefficient are critical at 95 °C and not at 80 °C and rest of the parameters show similar behavior.

Table II. Summary of five most sensitive parameters affecting cell current at different operating conditions and uncertainties in their available values in literature. Parameters with similar sensitivity magnitudes are grouped together resulting in more than five sensitive parameters at several operating conditions. The uncertainty values are characterized as: low uncertainty- less than 10% uncertainty, medium- 10 to 50% uncertainty, and high- more than 50% uncertainty.

Operating condition	Most sensitive parameters	Sensitivity valuemagnitude range	Uncertainty in literature
80 °C, 150 kPa 40% RH, air	$\alpha_{c,ORR}$	1–6	Low
	λ_V	0–5	High
	$A_{v,c}$,$i_{0,c}$	0.25–1	Medium
	$H_{O_2,m}$, $\kappa_{m,V}$	0–0.85	Medium/High
	$\epsilon_{V,GDL}$, L_{cCL}, L_{mem}	0–0.75	Medium
80 °C, 150 kPa 80% RH, air	$\alpha_{c,ORR}$	0–5	Low
	λ_V	0–5	High
	$\epsilon_{V,GDL}$	0–3	Medium
	$A_{v,c}$,$i_{0,c}$	0.25–1	Medium
	$H_{O_2,m}$, $\kappa_{m,V}$	0–0.85	Medium/High
80 °C, 150 kPa 80% RH, 5% O_2	$\alpha_{c,ORR}$	0–6	Low
	λ_V	0–5	High
	$\epsilon_{V,GDL}$	0–4	Medium
	$A_{v,c}$, $i_{0,c}$, γ_{O_2}	0–1.5	Medium
	$\beta_{\tau,GDL}$	0–1.1	Medium
80 °C, 150 kPa 100% RH, air	$S_{L,CL}$	0–40	High
	θ_m	0–30	Medium
	$\alpha_{c,ORR}$	0–6	Low
	$\epsilon_{V,GDL}$	0–3.5	Medium
	$\beta_{\tau,GDL}$	0–3	Medium
95 °C, 250 kPa 80% RH, air	$\alpha_{c,ORR}$	0–5	Low
	λ_V	0–5	High
	$\epsilon_{V,GDL}$	0–4	Medium
	$A_{v,c}$, $i_{0,c}$, $i_{0,a}$	0.25–1	Medium
	$H_{O_2,m}$, $\kappa_{m,V}$, L_{cCL}	0–0.85	Medium/High

Furthermore, given that heavy duty vehicles usually operate at higher cell potential ($E_{cell} \simeq 0.8V$) for increased efficiency, the output parameters of interest in Fig. 7 are the ones at 0.8 V. In terms of design parameters, it can be seen that cathode and anode ECSA, ionomer water uptake and conductivity, oxygen dissolution in ionomer ($H_{O_{2,m}}$), thickness of cathode catalyst layer and membrane, and cell humidity can be manipulated to get the largest impact on cell performance at 0.8 V. A cost, power, and efficiency optimization can be easily done using this small set of crucial parameters at conditions relevant to heavy duty vehicles.

While the detailed analysis above looked at the impact of model parameters on several outputs, in most experimental conditions only the cell performance (polarization behavior) is usually measured. Therefore, to summarize the study, five parameters were identified at each operating condition that exhibit the maximum impact on cell current density as given in Table II. Parameters with similar sensitivity magnitudes are grouped together. The uncertainty in available values of these parameters in literature is also summarized based on summary by Vetter and Schumacher.[24] It can be observed in Table II that several parameters can impact the model outputs significantly, although the most sensitive parameters vary between operating conditions. Given that in an integral cell (low-stoichiometry real-life operation) many of the operating conditions can be encountered along the flow path,[18] all of these parameters can be critical for determining and optimizing overall cell performance. Furthermore, cell parameters such as thicknesses, ECSA, ionomer fractions, saturation etc can also change during cell operation due to catalyst coarsening, carbon corrosion and other mechanisms. Therefore, this sensitivity analysis can also be critical to understand the durability and aging behavior of a cell. These observations are different from the ones made by Vetter and Schumacher[41] where they determined only the membrane properties to be of main importance. This is primarily due to the fact that the model used by Vetter and Schumacher[41] uses a simple 1-D model, which doesn't take into account land/channel effects, along-the-channel effects, Schroeder's paradox,[48] and detailed reaction kinetics. Furthermore, unlike current work, the study by Vetter and Schumacher[41] did not consider varying operating conditions. The recent work by Goshtasbi, et al.[21] however, also shows high sensitivity predictions for some of the other parameters identified in this study, especially for cathode kinetics parameters and effective diffusivities of different layers. Even though the study by Goshtasbi, et al.[21] uses a less rigorous MEA model, it does take into account most of the physics. Furthermore, it is a transient model which also accounts for along-the-channel effects resulting in it being more sensitive to stoichiometry, pressure and porous layer properties compared to current work. Overall, it is observed that regardless of the framework, some parameters show similar sensitivities in different studies, e.g., membrane properties are crucial in all frameworks. In our opinion, this is due to the fact that all the modeling frameworks rely on the same conservation and transport equations. Therefore, even though some models have simpler physics, they may still be useful to predict parameter sensitivity; albeit in a more local sense compared to a more detailed physical model which can estimate the sensitivities in a more global manner.

It can be seen in Table II that all the sensitive parameters except cathode transfer coefficient have medium to high uncertainty in available literature values. Therefore, it is even more crucial to direct future experimental studies towards measuring these properties with high accuracy and certainty. Finally, properties such as permeability of different layers, MPL saturation properties, rate of evaporation and channel heat transfer show almost negligible impact on model outputs at all operating conditions, making them the least significant parameters in this framework. It must be noted however, that these parameters are less impactful only in this framework under steady-state conditions. The sensitivity of cell parameters maybe different in another framework or in transient conditions.

The sensitivity analysis is not only useful for understanding which parameters are most significant and need to be measured accurately, it can also be used to shortlist design and optimization parameters. The most sensitive parameters are also the ones which can impact the cell's performance the most and therefore can be selectively manipulated to optimize performance. While several of the parameters identified in Table II cannot be changed easily (e.g., transfer coefficient and exchange current density) most of them can be manipulated by changing fuel cell geometry, ionomer material, catalyst loading, porous materials, and operating conditions. This study provides a manageable set of crucial parameters at each operating condition which can be used for fast cell optimization.

A major issue in parameter uncertainty analysis is the high correlation between certain parameters. Two parameters are said to be correlated when they impact the model outputs in the same way, i.e., the sensitivity profiles are the same, which is also noted by Goshtasbi et al.[21] For example, exchange current density and catalyst specific area always appear as a product. Therefore, it is not possible to deconvolute their individual uncertainty impacts. Looking at the sensitivity profiles of cell current density with respect to different parameters, several of the sensitivity profiles look similar. For example, most of the ionomer properties impact the ohmic losses in the cell and therefore have similar impact. Relying only on cell polarization performance alone can be therefore problematic for parameter identification and data fitting. However, the parameters that show similar sensitivity to current density, may exhibit different sensitivity to other model outputs, thereby making their effects discernible. It is therefore advisable to experimentally measure other cell characteristics as well. While variables such as membrane hydration and overpotential can be difficult to measure, properties such as outlet temperature, high frequency resistance (HFR) and outlet liquid flow rate can be used for deconvoluting the effects of different parameters and identifying them. The sensitivity analysis can further benefit in parameter identification and fitting by identifying the parameters that are most likely to affect the model output and eliminating non-consequential parameters from fitting.

Conclusions

This article presented a comprehensive parameter sensitivity analysis using a multiphysics 2-D MEA model. The PEMFC model used in this article is physically and mathematically more robust than used in previous similar studies. An uncertainty propagation analysis was used to estimate the sensitivity of 21 model outputs to nearly 50 model input parameters. The analysis was performed at multiple operating conditions to encompass several possible conditions that can be encountered in PEMFC operation.

It was observed that the most crucial parameters of the model are different for each operating condition. While at non-flooded (RH $<$ 100%) conditions, cathode kinetics and membrane-ohmic-loss related parameters are critical; gas transport and porous-media saturation behavior are more crucial at fully humidified conditions. Several of these identified parameters, such as cathode exchange current density, membrane water uptake, membrane conductivity and GDL tortuosity have significant uncertainty associated in literature values. This makes them prime candidates for focused experimental efforts, which can lead to better model prediction capabilities. The sensitivity analysis can also help in improving data-fitting by deconvoluting correlated parameters and by eliminating redundant parameters from the fitting. An understanding of most crucial parameters can also help with designing stack-level control systems, material design for desired properties and to identify crucial aging and durability behavior of the cell. Finally, a knowledge of the crucial cell parameters at each operating condition provides ways for fast optimization and for designing better PEFCs.

While this study encompassed several parameters and operating conditions, it still remains a local sensitivity study. Due to this,

several parameters which are only crucial in certain operating conditions, or potentials, or parameter combinations may not have been identified. Furthermore, the impact of the identified crucial parameters maybe different in a full 3-D model at low stoichiometry where operating conditions continuously change along the channel. Performing a truly global sensitivity or a local sensitivity analysis on a 3-D model is currently infeasible as the computation times will be impractical. Efforts are currently underway to develop more efficient data-driven PEMFC models, which can be then used for these detailed studies.

Acknowledgments

The authors would like to thank Matthias Hanauer and Giovanna Bucci at Bosch for their valuable suggestions. The authors would also like to thank Andrew Crothers at LBNL for his suggestions on data visualization. The authors thank funding via a research gift from Robert Bosch and subsequent funding for additional simulations and analysis and writing from the Million Mile Fuel Cell Truck (M^2FCT) Consortium, funded by the DOE EERE Hydrogen and Fuel Cell Technologies Office under contract number DE-AC02-05CH11231 (LBNL).

Disclaimer

Appendix

Table A·I. List of input parameters and parameter ranges for sensitivity analysis. All input parameters except the operating conditions and geometric parameters retain their basic functional forms and are varied using pre-factor k ($k = f/f^{ref}$). The values provided in this table are all pre-factors, except the operating conditions and geometric parameters, which are the actual values of the input parameters.

Parameter class	Input parameter	Parameter name	Minimum value	Maximum value	Scaling
Operating conditions	T_{cell}	Cell temperature (Celsius)	50	90	Linear
	$RH = RH_{ca}$	Anode/cathode humidity	0.4	0.9	Linear
Geometric parameters	$\beta_{\tau,G,GDL}$	Bruggeman tortuosity exponent for GDL	0.5	4	Linear
	$\beta_{\tau,G,MPL}$	Bruggeman tortuosity exponent for MPL	0.5	4	Linear
	$\beta_{\tau,G,aCL}$	Bruggeman tortuosity exponent for anode CL	0.5	3	Linear
	$\beta_{\tau,G,cCL}$	Bruggeman tortuosity exponent for anode CL	0.5	3	Linear
	$\epsilon_{v,GDL}$	Void volume fraction for GDL	0.5	0.9	Linear
	$\epsilon_{v,MPL}$	Void volume fraction for MPL	0.45	0.8	Linear
	$\epsilon_{v,aCL}$	Void volume fraction for anode CL	0.3	0.75	Linear
	$\epsilon_{v,cCL}$	Void volume fraction for cathode CL	0.3	0.75	Linear
	$\epsilon_{m,agg}$	Ionomer volume fraction in agglomerate core	0.1	0.75	Linear
	$\epsilon_{m,aCL}$	Ionomer volume fraction in anode CL	0.06	0.3	Linear
	$\epsilon_{m,cCL}$	Ionomer volume fraction in cathode CL	0.06	0.3	Linear
	L_{GDL}	GDL thickness (μm)	50	400	Linear
	L_{MPL}	MPL thickness (μm)	10	100	Linear
	L_{aCL}	Anode CL thickness (μm)	0.5	20	Linear
	L_{cCL}	Cathode CL thickness (μm)	0.5	20	Linear
	L_{mem}	Membrane thickness (μm)	1	75	Linear
Kinetics parameters pre-factor	$i_{0,a}A_{v,a}$	Anode (Exchange current density x Catalyst specific area)	0.001	10	Log
	$i_{0,c}A_{v,c}$	Cathode (Exchange current density x Catalyst specific area)	0.001	10	Log
	$\alpha_{a,HOR}$	Anodic transfer coefficient for hydrogen oxidation reaction	0.4	1.1	Linear
	$\alpha_{c,HOR}$	Cathodic transfer coefficient for hydrogen oxidation reaction	0.4	1.1	Linear
	$\alpha_{c,ORR}$	Cathodic transfer coefficient for oxygen reduction reaction	0.8	2.2	Linear
	γ_{H_2}	Hydrogen reaction order	0.45	1	Linear
	γ_{O_2}	Oxygen reaction order	0.45	1	Linear
Saturation properties pre-factor	$S_{L,GDL}$	Liquid saturation in GDL	0.75	1.25	Linear
	$S_{L,MPL}$	Liquid saturation in MPL	0.75	1.25	Linear
	$S_{L,CL}$	Liquid saturation in CL	0.75	1.25	Linear
Agglomerate prop. pre-factor	δ_{agg}	Ionomer film thickness on agglomerate	0.25	5	Linear
	r_{agg}	Agglomerate radius	0.2	2	Linear
Ionomer properties pre-factor	λ_V	Equilibrium water vapor uptake in ionomer	0.2	1.2	Linear
	$r_{pore,m}$	Average pore radius in ionomer	0.1	10	Log
	$\theta_{w,m}$	Contact angle of water in ionomer	1	1.1	Linear
	$k_{V,m}$	Vapor adsorption/desorption constant in ionomer	0.012	10	Log
	$k_{L,m}$	Liquid adsorption/desorption constant in ionomer	0.01	10	Log
	k_{ev}	Evaporation/condensation rate in pores	0.001	10	Log
	$H_{O_2,m}$	Henry's constant for oxygen dissolution in ionomer	0.1	10	Log
	$D_{O_2,m}$	Oxygen diffusivity in ionomer	0.1	10	Log
	$k_{T,GDL}$	Thermal conductivity of GDL	0.1	10	Linear

Table A·I. (Continued).

Parameter class	Input parameter	Parameter name	Minimum value	Maximum value	Scaling
	$k_{T,MPL}$	Thermal conductivity of MPL	0.1	10	Linear
	$k_{T,CL}$	Thermal conductivity of CL	0.1	10	Linear
	$k_{T,m}$	Thermal conductivity of membrane	0.1	10	Linear
	$\kappa_{m,L}$	Liquid equilibrated membrane proton conductivity	0.1	10	Log
Transport properties pre-factor	$\kappa_{m,V}$	Vapor equilibrated membrane proton conductivity	0.1	10	Log
	$\alpha_{m,L}$	Liquid equilibrated membrane water diffusivity	0.1	10	Log
	$\alpha_{m,V}$	Vapor equilibrated membrane water diffusivity	0.1	10	Log
	$\xi_{m,L}$	Liquid equilibrated membrane electroosmotic coefficient	0.5	2	Linear
	$k_{0,GDL}$	Absolute permeability of GDL	0.1	10	Log
	$k_{0,MPL}$	Absolute permeability of MPL	0.1	10	Log
	$k_{0,CL}$	Absolute permeability of CL	0.1	10	Log
	h_{cool}	Convective heat transfer coefficient between coolant and plate	0.1	10	Log
	h_{chan}	Convective heat transfer coefficient between channel and plate	0.1	10	Log
	p_{thru}	GDL liquid breakthrough pressure	0.25	2.5	Linear
	k_L	GDL/channel liquid breakthrough flux coefficient	0.001	10	Log

ORCID

Lalit M. Pant https://orcid.org/0000-0002-0432-3902
Adam Z. Weber https://orcid.org/0000-0002-7749-1624

References

1. D. Papageorgopoulos, "Fuel Cell R&D Overview."*DOE 2019 Annual Merit Review and Peer Evaluation Meeting*, Crystal City, VA, USA (U. S. Department of Energy, EERE) (2019).
2. A. Z. Weber et al., *J. Electrochem. Soc.*, **161**, F1254 (2014).
3. A. Z. Weber and J. Newman, *Chem. Rev.*, **104**, 4679 (2004).
4. M. Secanell, J. Wishart, and P. Dobson, *JPS*, **196**, 3690 (2011).
5. D. M. Bernardi and M. W. Verbrugge, *AIChE*, **37**, 1151 (1991).
6. T. E. Springer, T. A. Zawodzinski, and S. Gottesfeld, *J. Electrochem. Soc.*, **138**, 2334 (1991).
7. M. Eikerling and A. A. Kornyshev, *J. Electroanal. Chem.*, **453**, 89 (1998).
8. C. Y. Wang, W. B. Gu, and B. Y. Liaw, *J. Electrochem. Soc.*, **145**, 3407 (1998).
9. A. Z. Weber, *Modeling Water Management In Polymer -Electrolyte Fuel Cells* (University of California, Berkeley) (2004).
10. D. Natarajan and T. V. Nguyen, *J. Electrochem. Soc.*, **148**, A1324 (2001).
11. W. Sun, B. A. Peppley, and K. Karan, *Electrochim. Acta*, **50**, 3359 (2005).
12. G. Lin and T. V. Nguyen, *J. Electrochem. Soc.*, **153**, A372 (2006).
13. R. J. Balliet and J. Newman, *J. Electrochem. Soc.*, **158**, B927 (2011).
14. L. Xing, X. Liu, T. Alaje, R. Kumar, M. Mamlouk, and K. Scott, *Energy*, **73**, 618 (2014).
15. I. V. Zenyuk, P. K. Das, and A. Z. Weber, *J. Electrochem. Soc.*, **163**, F691 (2016).
16. S. Um and C. Y. Wang, *JPS*, **125**, 40 (2004).
17. A. A. Kulikovsky, *J. Electrochem. Soc.*, **150**, A1432 (2003).
18. L. M. Pant, M. R. Gerhardt, N. Macauley, R. Mukundan, R. L. Borup, and A. Z. Weber, *Electrochim. Acta*, **326**, 134963 (2019).
19. M. Moore, A. Putz, and M. Secanell, *J. Electrochem. Soc.*, **160**, F670 (2013).
20. L. M. Pant and A. Z. Weber, *J. Electrochem. Soc.*, **164**, E3102 (2017).
21. A. Goshtasbi, J. Chen, J. R. Waldecker, S. Hirano, and T. Ersal, *J. Electrochem. Soc.*, **167**, 044504 (2020).
22. A. Kravos, D. Ritzberger, C. Hametner, S. Jakubek, and T. Katrašnik, *IJHE*, **46**, 13832 (2020).
23. A. Kravos, D. Ritzberger, G. Tavčar, C. Hametner, S. Jakubek, and T. Katrašnik, *JPS*, **454**, 227930 (2020).
24. R. Vetter and J. O. Schumacher, *JPS*, **438**, 227018 (2019).
25. A. P. Schmidt, M. Bitzer, Á. W. Imre, and L. Guzzella, *JPS*, **195**, 5071 (2010).
26. L. Zhang, C. Lyu, G. Hinds, L. Wang, W. Luo, J. Zheng, and K. Ma, *J. Electrochem. Soc.*, **161**, A762 (2014).
27. A. M. Bizeray, J. H. Kim, S. R. Duncan, and D. A. Howey, *IEEE Trans. Control Syst. Technol.*, **27**, 1862 (2019).
28. B. Carnes and N. Djilali, *JPS*, **144**, 83 (2005).
29. Q. Guo, V. A. Sethuraman, and R. E. White, *J. Electrochem. Soc.*, **151**, A983 (2004).
30. J. M. Correa, F. A. Farret, V. A. Popov, and M. G. Simoes, *ITEnC*, **20**, 211 (2005).
31. A. Mawardi and R. Pitchumani, *JPS*, **160**, 232 (2006).
32. W. Q. Tao, C. H. Min, X. L. Liu, Y. L. He, B. H. Yin, and W. Jiang, *JPS*, **160**, 359 (2006).
33. C. H. Min, Y. L. He, X. L. Liu, B. H. Yin, W. Jiang, and W. Q. Tao, *JPS*, **160**, 374 (2006).
34. L. Placca, R. Kouta, J.-F. Blachot, and W. Charon, *JPS*, **194**, 313 (2009).
35. S. S. Araya, S. J. Andreasen, and S. K. Kær, "Parametric Sensitivity Tests — European PEM Fuel Cell Stack Test Procedures." *ASME 2014 12th International Conference on Fuel Cell Science, Engineering and Technology*, Boston, Massachusetts, USA, June 30–July 2 (2014), V001T06A006.
36. M. Noorkami, J. B. Robinson, Q. Meyer, O. A. Obeisun, E. S. Fraga, T. Reisch, P. R. Shearing, and D. J. L. Brett, *IJHE*, **39**, 1439 (2014).
37. G. Correa, F. Borello, and M. Santarelli, *IJHE*, **40**, 10354 (2015).
38. N. Noguer, D. Candusso, R. Kouta, F. Harel, W. Charon, and G. Coquery, *IJHE*, **40**, 3968 (2015).
39. D. Zhao, F. Gao, P. Massonnat, M. Dou, and A. Miraoui, *ITEnC*, **30**, 1008 (2015).
40. B. Laoun, M. W. Naceur, A. Khellaf, and A. M. Kannan, *IJHE*, **41**, 9521 (2016).
41. R. Vetter and J. O. Schumacher, *JPS*, **439**, 126529 (2019).
42. A. Goshtasbi, J. Chen, J. R. Waldecker, S. Hirano, and T. Ersal, *J. Electrochem. Soc.*, **167**, 044505 (2020).
43. L. M. Pant, Z. Yang, M. L. Perry, and A. Z. Weber, *J. Electrochem. Soc.*, **165**, F3007 (2018).
44. M. Moore, P. Wardlaw, P. Dobson, J. J. Boisvert, A. Putz, R. J. Spiteri, and M. Secanell, *J. Electrochem. Soc.*, **161**, E3125 (2014).
45. D. A. Belsley, E. Kuh, and R. E. Welsch, *Regression Diagnostics: Identifying Influential Data and Sources of Collinearity* (Wiley, New York, NY) (1980).
46. L. N. Trefethen and D. Bau III, *Numerical Linear Algebra* (SIAM, Philadelphia, PA) (1997).
47. *Fuel Cell Technical Team Roadmap* (US DOE Office of Energy Efficiency and Renewable Energy (EERE), Vehicle Technologies Office) (Washington, DC, USA) (2013).
48. A. Z. Weber and J. Newman, *J. Electrochem. Soc.*, **150**, A1008 (2003).